

UC Irvine

UC Irvine Previously Published Works

Title

Dysfunction of the aging female mouse urethra is associated with striated muscle loss and increased fibrosis: an initial report.

Permalink

<https://escholarship.org/uc/item/3b12v9px>

Journal

American Journal of Clinical and Experimental Urology, 11(6)

ISSN

2330-1910

Authors

Sadeghi, Zhina

Wu, Yi Xi

Vu, Amberly

et al.

Publication Date

2023

Peer reviewed

Original Article

Dysfunction of the aging female mouse urethra is associated with striated muscle loss and increased fibrosis: an initial report

Zhina Sadeghi^{1,2*}, Yi Xi Wu^{1*}, Amberly Vu¹, Liankun Song¹, William Phan³, Jeffery Kim^{4,5}, Janet R Keast⁶, Ulysses Balis⁷, John DeLancey⁸, S Armando Villalta^{2,9}, Xiaolin Zi^{1,10}

¹Department of Urology, University of California, Irvine, CA 92868, USA; ²Muscle Biology and Disease Research Center, University of California, Irvine, CA 92868, USA; ³Department of Cell Biology and Neuroscience, University of California, Riverside, CA 92521, USA; ⁴Department of Pathology and Laboratory Medicine, University of California, Irvine, CA 92868, USA; ⁵Experimental Tissue Resource, University of California, Irvine, CA 92868, USA; ⁶Department of Anatomy and Physiology, University of Melbourne, Parkville, VIC 3010, Australia; ⁷Department of Pathology-Bioinformatics, University of Michigan, Ann Arbor, MI 48109, USA; ⁸Department of Gynecology, University of Michigan, Ann Arbor, MI 48109, USA; ⁹Department of Physiology and Biophysics, University of California, Irvine, CA 92868, USA; ¹⁰Veterans Affairs Long Beach Healthcare System, Long Beach, CA 90822, USA. *Equal contributors.

Received September 21, 2023; Accepted September 29, 2023; Epub December 15, 2023; Published December 30, 2023

Abstract: The decline of urethral function with advancing age plays a major role in urinary incontinence in women, impairing quality of life and economically burdening the health care system. However, none of the current urinary incontinence treatments address the declining urethral function with aging, and the mechanisms by which aging impacts urethra physiology remain little known or explored. Here, we have compared functional, morphometric, and global gene expression of urethral tissues between young and old female mice. Bladder leak point pressure (LPP) measurement showed that the aged female mice had 26.55% lower LPP compared to younger mice. Vectorized Scale-Invariant Pattern Recognition (VIPR) analysis of the relative abundance of different tissue components revealed that the mid-urethra of old female mice contains less striated muscle, more extracellular matrix/fibrosis, and diminished elastin fibers ratio compared to young mice. Gene expression profiling analysis (bulk RNA-seq of the whole urethra) showed more down-regulated genes in aged than young mice. Immune response and muscle-related (striated and smooth) pathways were predominantly enriched. In contrast, keratinization, skin development, and cell differentiation pathways were significantly downregulated in aged urethral tissues compared to those from young female mice. These results suggest that molecular pathways (*i.e.*, ACVR1/FST signaling and CTGF/TGF- β signaling) leading to a decreased striated muscle mass and an increase in fibrous extracellular matrix in the process of aging deserve further investigation for their roles in the declined urethral function.

Keywords: Urethral striated muscle, aging, urinary incontinence, fibroadipogenic cells

Introduction

The prevalence of urinary incontinence in women is up to 60%, rises with aging, costs nearly 10 billion dollars annually, and is associated with a substantial decrease in health-related quality of life [1]. While only 25-61% of symptomatic community-dwelling women seek care, success for current treatment strategies targeting the bladder muscle dysfunction in urgency urinary incontinence and urethra sup-

port in stress urinary incontinence has plateaued at levels that leave many treated females with continued incontinence [2-4]. Moreover, complications of current urethral support treatments, such as urinary outlet obstruction and mesh erosion, have harmful impacts on patients' quality of life [5]. While urethral function is one of the key factors responsible for stress and urgency urinary incontinence, none of the current urinary incontinence treatments fully address female urethral failure.

Investigating age-derived urethral dysfunction

Aging plays a crucial role in the decline of urethral function, resulting in urinary incontinence. A prior epidemiological study in nulliparous women demonstrated that age alone explains about 57% of the decrease in female urethral function indicated as a decline in maximum urethral closure pressure (MUCP). This study found that MUCP declines 15 cmH₂O every decade with increasing age [6]. Another study evaluated the MUCP of 169 healthy female cohorts composed of children to older females; it demonstrated that 21- to 25-year-old women have 25% and 50% higher MUCP than 36- to 40-year-old and 61- to 65-year-old, respectively [7]. Unfortunately, few studies have investigated why urethral function declines and the tissue changes associated with senescence.

Previous work by Carlile *et al.* showed a 50% decrease in urethral striated muscle cell count between 20- and 80-year-old [8]. The reduction in striated muscle cell number is one of the changes suggested to contribute to this MUCP decline, thus resulting in urethral function decline. However, further investigation of the effects of aging on urethra physiology is still needed. To evaluate the impact of aging on urethra tissues, we utilized an animal model to investigate the changes in urethral muscles. The commercial availability of inbred aged mice models and well-established mouse genomics make this an ideal species to evaluate age-associated changes in urethra. To our knowledge, no comprehensive gene expression analysis has been performed on the female urethra in the context of aging. In this study, we focused on the impact of aging on functional, morphometric, and gene expression changes in the urethra of female mice. In summary, our study revealed several changes in the mid-urethra of aged female mice, including lower leak point pressure (LPP), less striated muscle, more extracellular matrix/fibrosis, and diminished elastin. Transcriptome analysis of the urethra showed more down-regulated genes in older mice than in younger mice, while the differential gene expression analysis suggested an enrichment of muscle process, contraction, and immune response.

Materials and methods

All animals (C57BL/6) were purchased from Jackson Laboratory (Bar Harbor, ME, USA) under a UC Irvine-approved IACUC protocol.

DNA primers were synthesized and obtained from Integrated DNA Technologies (Coralville, IA, USA). Unless specified otherwise, all other chemicals used were obtained from Sigma-Aldrich (St. Louis, MO, USA).

Leak point pressure measurement

For measuring leak point pressure (LPP) as evidence of urethral resistance against urinary leakage, a modified method of Liu *et al.* was used [9]. Four young (14-week) and three aged (84-week) mice were intraperitoneally anesthetized under urethane (1.2 g/kg body weight) and xylazine (10 mg/kg body weight). In the supine position, a midline incision was made until the bladder dome was exposed. A suprapubic bladder catheter (20-gauge × 2-inch Angio catheter) was connected to the bladder dome and secured with a 3-0 Vicryl suture to the dome. The bladder catheter was connected to a pressure transducer and data acquisition system (MP150, BIOPAC systems, Inc., CA, USA) and flow pump (Genie Touch, Kent Scientific, CT, USA). Each mouse underwent an adjustment period of filling (10 ml/hr) and spontaneous voiding. After spontaneous voiding, if the bladder still contained urine, it was emptied using a Crede maneuver to confirm the bladder pressure returning to 0.0 cmH₂O. The bladder was then filled with saline at a rate of 1 ml/hr; the bladder pressure was carefully monitored until the mouse leaked a drop of saline via the urethra. When leakage was visualized from the urethra, the pump was rapidly stopped, and bladder pressure immediately dropped with no further leakage. The peak bladder pressure at the time of the leak was defined as bladder LPP. The bladder was then emptied with the Crede maneuver to reach back to 0.0 cmH₂O. The bladder LPP test was conducted thrice with each mouse, and the mean ± standard deviation was calculated. Cervical dislocation under urethane induced anesthesia were performed to humanely euthanized the animals post bladder LPP test.

Histological staining of mouse urethra and tissue quantification

Two aged (94-week) and two young (14-week) female mice had their bladder transected from the urethra at bladder neck level after isoflurane-induced anesthesia, followed by cervical dislocation to ethically killed the mouse. The

Investigating age-derived urethral dysfunction

dissected whole urethras were fixed in 10% formalin for 12 hours, followed by washing with phosphate buffered saline (PBS), preserved in 70% ethanol, and sent to the UC Irvine Experimental Tissue Core for post-processing. The formalin-fixed urethra tissue was divided into two equal-length parts (the length of each part of the urethra was 3.5-5.0 mm, depending on the size of the mouse). The equal-length pieces of urethra were orientated parallel to each other in the same paraffin block, with the mid-urethra facing the same direction. Serial 4- μ m paraffin embedded mid-urethra transverse sections were obtained from the mid-urethral side and stained with Masson's Trichrome (collagens) and Vernhoeff-Van Gieson's (VVG) (elastin) using conventional histology methods. Stained slides were scanned at histological resolution at 40 \times magnification. Quantitative analysis was conducted on the striated muscle (StM) layer of the mid-urethra. Vectorized scale-Invariant Pattern Recognition (VIPR) was used to identify StM, extracellular matrix and connective tissue, and elastin components of the urethral wall using a computational image pipeline that transforms each image location into a local kernel figure-of-merit heatmap for cell type, using K-Means clustering followed by boosting with early cuts [10, 11]. The StM layer area of interest was extracted and fractionated by 100-pixel wide sliding window color gating along the urethral luminal axis. This enabled the calculation of the proportion comprised of each primary tissue type at the mid-urethral level.

Immunofluorescence staining of mice urethra

For immunohistochemistry, tissue samples were acquired by the method above and the method of Smith-Anttila *et al.* was used [12], modified to include an antigen retrieval step. In short, the slides were incubated with fresh proteinase K solution, followed by heating in 94.0°C citrate buffer (pH 9.0) for 10 minutes for retrieval. Sections were washed in PBS and incubated for 1 h at room temperature with PBS containing 10% non-immune horse serum and 0.1% Triton X-100. Sections were washed and incubated at room temperature for 18-24 h with the primary antibody Platelet-derived Growth Factor Receptor alpha (PDGFR- α) (Biotechne, MN, USA), goat anti-mouse, diluted in hypertonic PBS (PBS containing 17 g NaCl per liter). Slides were washed in PBS before being

incubated with Alexa Fluor® (AF) secondary antibodies: donkey anti-goat AF647 (Jackson ImmunoResearch Lab, PA, USA) diluted 1:1000 in hypertonic PBS, for 2.5 h at room temperature. Then, slides were washed in PBS, incubated with 4,6-diamidino-2-phenylindole (DAPI), washed in PBS, and mounted in buffered glycerol. Images were captured with a Keyence BZ-X 710 fluorescence microscope and camera. Where required, minor adjustments were made in images using Adobe Photoshop to ensure close matching to labeling as viewed directly down the microscope. A minimum of three non-consecutive sections per sample were examined.

Isolation of total RNA from tissue

At the selected experimental age (14 or 94 weeks), the female mouse urethras were collected (n = 3 per group); mice were euthanized using cervical dislocation under isoflurane-induced anesthesia, with the aim to decrease pain and animal distress. The entire length of the urethra from bladder neck to the meatus was excised in sterile condition and preserved using RNALater (Thermo Fisher Scientific, Waltham, MA, USA) and stored at -20°C until used.

Total RNA was extracted using Invitrogen PureLink RNA Mini kit (Thermo Fisher Scientific, Waltham, MA, USA). The tissues were homogenized using a pellet pestle (Fisher Scientific, Hampton, NH, USA) followed by centrifuge-assisted homogenizers (Thermo Fisher Scientific, Waltham, MA, USA) to help further break down the tissues. PureLink DNase Set (Thermo Fisher Scientific, Waltham, MA, USA) was used to remove DNA material, following the manufacturer's instructions. A final volume of 35.0 μ L was eluted. RNA purity (ratio > 1.8 for UV absorbance of 260/280 nm) and quantity were determined using a spectrophotometer (EzDrop1000, Blue Ray Biotech, Xindian District, New Taipei City, Taiwan).

RNA sequencing

Zymo-Seq RiboFree Total RNA Library Kit (Zymo Research, Irvine, CA, USA) was used to prepare the final cDNA library for next-generation sequencing. In short, the isolated total RNA was reverse-transcribed to DNA using a mixture of poly-T and random hexamers reverse-

Investigating age-derived urethral dysfunction

transcription primers. The resulting DNA products were purified according to Zymo kit instructions; PCRs were performed to enrich and barcode to generate the final Illumina-compliant libraries. The quality and quantity of the libraries (Old = 3 and Young = 3) were evaluated by Bioanalyzer and Qubit. The UC Irvine Genomics Research and Technology Hub Core Facility sequenced the final library utilizing the MiSeq with 300-bp paired-end read to a depth of ~22 to 25 million reads per sample.

RNA-Seq analyses

CLC Genomic BenchWork (Qiagen, Hilden, Germany) was used to trim and quality control raw reads, followed by mapping to the mice genome, and finally, differential gene analysis was performed. Pathway enrichment analysis of the differential genes was performed using GSEA (Gene Set Enrichment Analysis). Differential genes with an absolute fold change of > 2 and a False Discovery Rate (FDR) of < 0.05 were used for pathway enrichment analysis.

Real-time reverse transcription-quantitative polymerase chain reaction (RT-qPCR)

Expression analysis of specific genes was done utilizing total RNA acquired by the aforementioned method. Targeted genes and their appropriate primers (Table S1) were obtained from various sources of publications, followed by checking primer specificity using the Basic Local Alignment Search Tool (BLAST) (blast.ncbi.nlm.nih.gov/Blast.cgi). One-step reverse transcription and quantitative PCR were performed using iTaq Universal Green One-Step RT-qPCR Kit (BioRad, CA, USA). RT-qPCR of specific genes was performed in a 96-well plate using a CFX Connect Real-Time System (BioRad, CA, USA).

Statistical analyses

Microsoft Excel 365 was used to collect experimental data. GraphPad Prism 9 was used for statistical data analysis and graph preparation. CLC Genomic BenchWork was used for statistical data analysis of RNA-seq data and figure preparation. Data were expressed as mean \pm standard deviation, and p -value < 0.05 was considered statistically significant for all experiments. FDR-value < 0.05 was considered statistically significant for the RNA-seq experiment.

Results

Bladder leak point pressure of mice urethra

Bladder leak point pressure (LPP) measurement demonstrated a slow rise to peak and rapid drop. The aged mouse group ($n = 3$) had an average (mean \pm SEM) LPP of 14.6 ± 1.3 cmH₂O, while the young mouse group ($n = 4$) had an average LPP of 19.8 ± 0.9 cmH₂O. The difference in LPP between the aged and young mouse group was found to be statistically significant, as shown in **Figure 1**.

Histological staining of mice urethra

VIPR analysis of the mid-urethral striated muscle layer demonstrated a lower percentage of StM in aged (38% and 31%) than young (47% and 50%) mice. Conversely, a higher proportion of the mid-urethra striated muscle layer tissue was represented by extracellular matrix connective-tissue (old and new) in aged (46% and 48%) than young (39% and 42%) mice, as shown in **Figure 2A** and **2C**. The proportion of tissue containing elastin was lower in aged (8% and 6%) than young (27% and 15%) mice as illustrated in **Figure 2B** and **2C**.

Transcriptomic analysis of aged vs. young female mice urethral tissue

To evaluate molecular alterations or changes of gene expression on urethra tissues with aging, we analyzed the transcriptome of aged (94 weeks) and young (14 weeks) female mice urethra tissues. Principal component analysis (PCA) revealed distinct differences in the transcriptomes corresponding with age (**Figure S1**), with 1,544 differentially expressed (DE) genes identified, as shown in **Figure 3**. All RNA-seq data was normalized to RPKM (Reads Per Kilobase per Million Mapped reads) prior to analysis. Compared to the younger urethral tissue, aged urethral tissue had more downregulated (962) than upregulated (582) genes, as shown in **Figure 3A**. The top ten upregulated genes observed in aged mice were *Tim4*, *pax5*, *cd22*, *Jchain*, *Lep*, *Pou2af1*, *Tnfrsf13c*, *Cd79a*, *Npr3*, and *Spib*, while the top downregulated genes observed were *Krt76*, *Krt16*, *Kprp*, *Krt6b*, *Dsc1*, *Dsg1a*, *Uox*, *Lor*, *Krtap3-3*, and *Slurp1*, see **Tables S2** and **S3** for the list of top 50 upregulated and downregulated genes. In the aged urethral tissue, many downregulated

Investigating age-derived urethral dysfunction

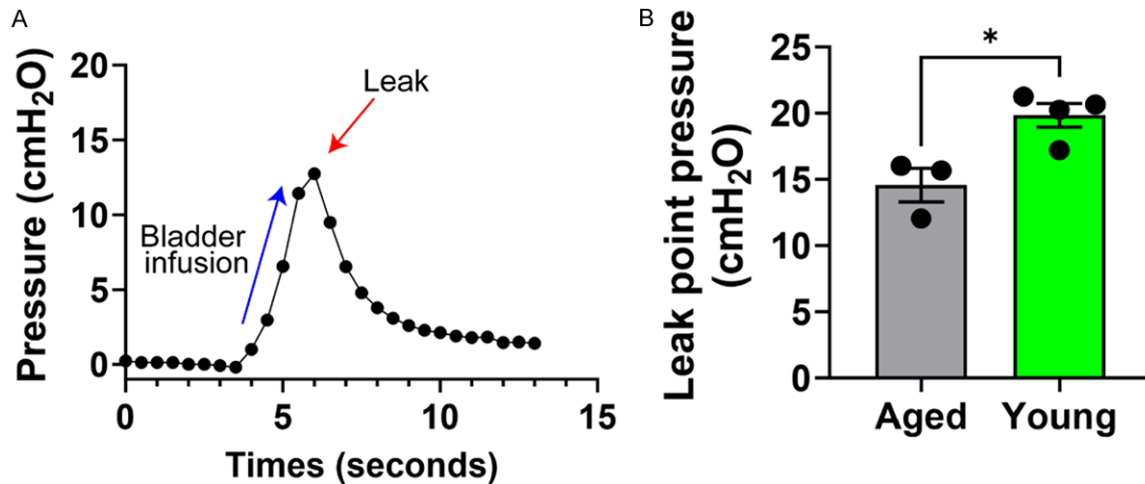


Figure 1. Peak voiding pressure in aged and young female mice. A. Example of bladder leak point pressure where the Black dots represent data points collected in 30 second increments, the Blue arrow illustrates the infusion of the bladder with fluid at 10 ml/hr, and the Red arrow indicates the leak point pressure (LPP) of the urethra. The Red arrow also indicates the stopping point for pump infusion. B. The average leak point pressure of aged and young mouse group is displayed. Each data point represents the LPP average of an individual mouse. The error bars indicate the SEM. The asterisk (*) denotes statistical significance based on the t-test ($P = 0.017$).

genes corresponded with keratin and skin development, such as *Krt16*, *Kprp*, and *Dsc*; however, many immune-associated and muscle-related genes, such as *Lep*, *Acvr1c*, and *Cxcl12*, were highly upregulated, as shown in **Figure 3B**. GSEA of the significant differential genes for biological processes showed similar results. Gene set enrichment showed an upregulated immune response and muscle-related (striated and smooth) pathways in aged urethral tissues, while keratinization, skin development, and cell differentiation pathways were significantly downregulated, as illustrated in **Figure 4**.

Reverse-transcriptase (RT)-quantitative polymerase chain reaction (qPCR) was used to further validate the genes differentially expressed between young and aged urethral tissues, from RNA-seq data. **Figure 5** shows that the expression of pro-myogenic and inflammation chemokines and cytokines *Cxcl12*, *Cxcl9*, *Il6*, *Osr1*, and *Il15* mRNA, was significantly higher in aged urethral tissues compared to those from young female mice ($P < 0.05$, student t-test). In addition, the aged urethral tissues from female mice exhibit increased expression of *Tgfb1*, *Ctgf*, and *Ly6a* (*Sca1*) mRNA compared to those from young mice. Tryptophan hydroxylase 1 (*Tph1*), the rate-limiting enzyme in the synthesis of peripheral serotonin, is also significantly

up-regulated in aged urothelial tissues ($P < 0.05$) [13].

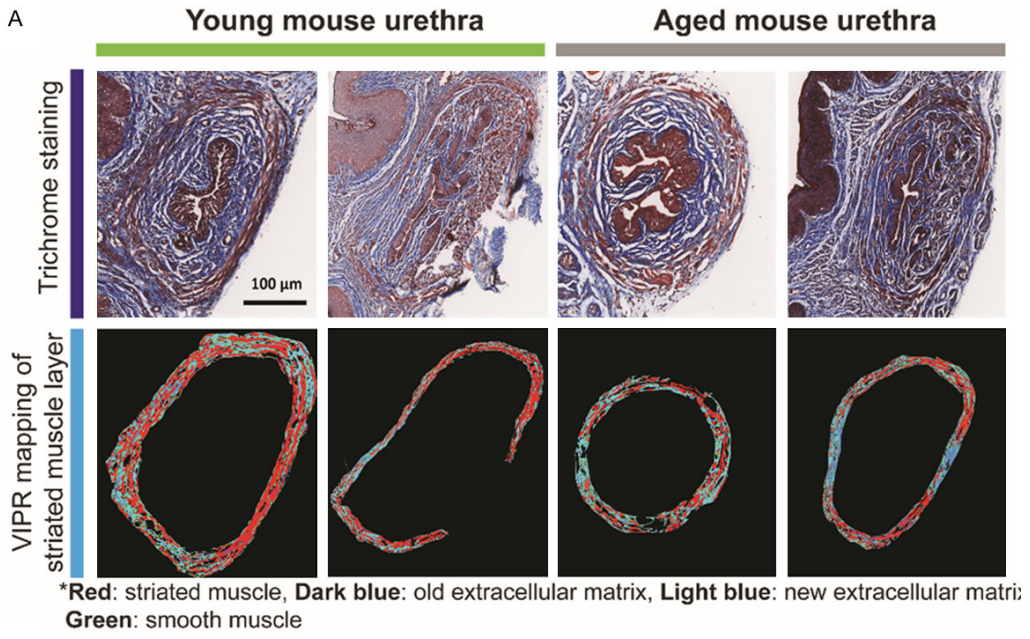
Immunofluorescence staining of mice urethra

Immunofluorescence staining of PDGFR- α - a cell surface tyrosine kinase receptor for growth factor families stimulating cells of mesenchymal origin with many studies suggest that this gene plays a role in organ development, wound healing, and tumor progression [14, 15] - in young and aged mice female urethral tissues and comparing them with their trichrome stained consecutive sections. The data demonstrated that PDGFR- α positive cells in the striated muscle layer of the urethra in both young and aged mice urethra (**Figure 6**).

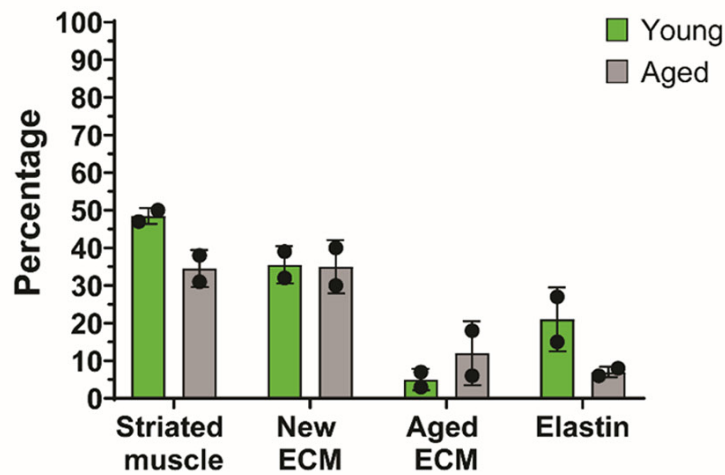
Discussion

Aging plays a crucial role in the decline of urethral function leading to urinary incontinence [6-8, 16]. As humans age, the number and density of urethral striated fibers decline with an average of 2-4% loss of striated fibers per year [17, 18]. In addition, elastic fibers in urethral tissues, which have been thought to contribute to the resting urethral pressure [17, 18], were found to decrease with aging. In this study, we have shown that the striated muscle layer of urethral tissues from aged female mice (94

Investigating age-derived urethral dysfunction



C **Tissue components within the striated muscle**



Investigating age-derived urethral dysfunction

Figure 2. VIPR analysis of female mouse urethral tissue. A. Ratio of striated muscle tissue, new and old ECM in the Trichrome stained striated muscle layer of mid-urethra. In the Trichrome, all ECM are stained blue; however, “old ECM” is depicted as acellular non-fibrillar dense aberrant tissue, whereas “new ECM” is characterized as a highly organized matrix with fibrillar components and structural integrity. Many ECM proteins have a long half-life (nearly decades), and they are prone to accumulate as tissues age, as such, they form areas of non-fibrillar dense, unorganized protein deposits - mainly composed of collagens and collagen-derivatives [41, 42]. B. Ratio of elastin in VVG stained striated muscle layer of mid-urethra. C. Comparison of ratio of striated muscle components in young and aged mice. The error bars represent standard deviations.

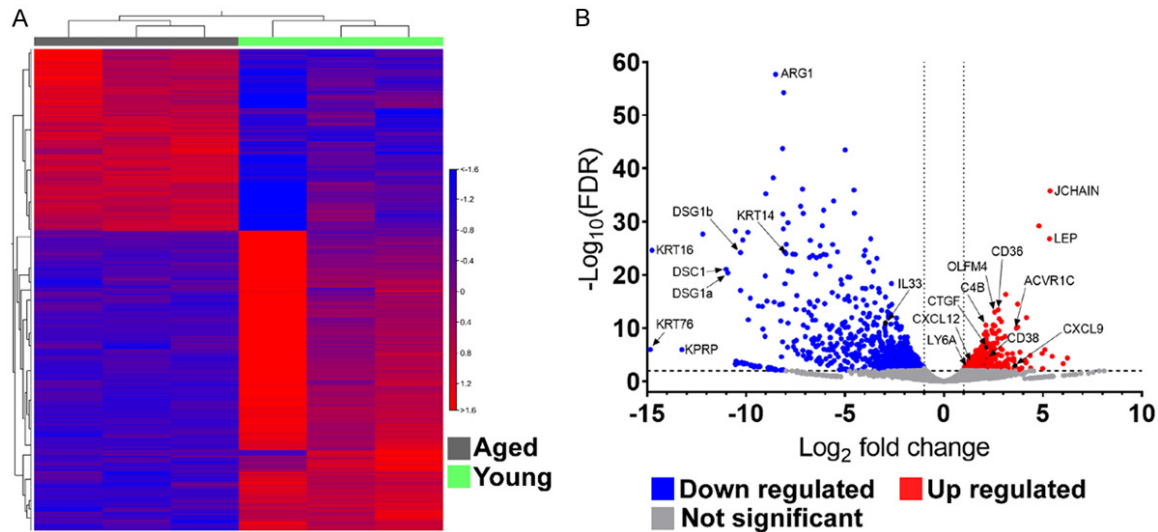


Figure 3. RNA-seq analysis of female mice urethra. A. Heatmap of differentially expressed genes between female aged (grey, $n = 3$) and young (green, $n = 3$) mice urethra tissue. Hierarchical clustering of 1,544 differentially expressed genes is shown (absolute fold change > 2 ; FDR $P \leq 0.01$). B. Volcano plot of significant differentially expressed genes. Blue represents the downregulated genes, Red represents the upregulated genes, and Grey represents no significant change in the aged versus young. Various forms of keratin and age-related genes are shown to be downregulated, while immune and muscle-related genes are upregulated in Aged versus Young mice urethra tissue.

weeks old) have lower proportion of striated muscles and elastin, but higher proportion of extracellular matrix connective-tissues than young mice (14 weeks old). These tissue architectural changes in aged female urethral tissues are highly consistent with previous findings on human aged female urethral tissues [8], which supports the use of experimental mice to model at least some key features and molecular changes in human urethra tissues and their aging.

LPP, the measurement of bladder pressure during urine leakage, provides an assessment of urethral resistance. Our result shows significantly decreased bladder LPP in aged mice compared to the young mice as evidence of reduced functional urethral resistance in aged mice compared to the young mice. This is consistent with a three-factor paradigm that emphasizes the role of decreased urethral

function as associated with lower urethral resistance with aging and is clinically associated with stress, urge, and mixed incontinence [19].

Currently, little is known about genomic alterations, in particular no report about gene expression profiling in the aged urethra of female mice or humans. We, therefore carried out whole transcriptome profiling analysis using an unbiased second-generation RNA sequencing method to create a global picture of gene expression between aged and young female mouse urethral tissues. The top enriched gene expression pathways include immune response and muscle-related (striated and smooth) pathways, whereas keratinization, skin development, and cell differentiation pathways were significantly downregulated in aged urethral tissues compared to those from female young mice. The significance of the RNA expression

Investigating age-derived urethral dysfunction

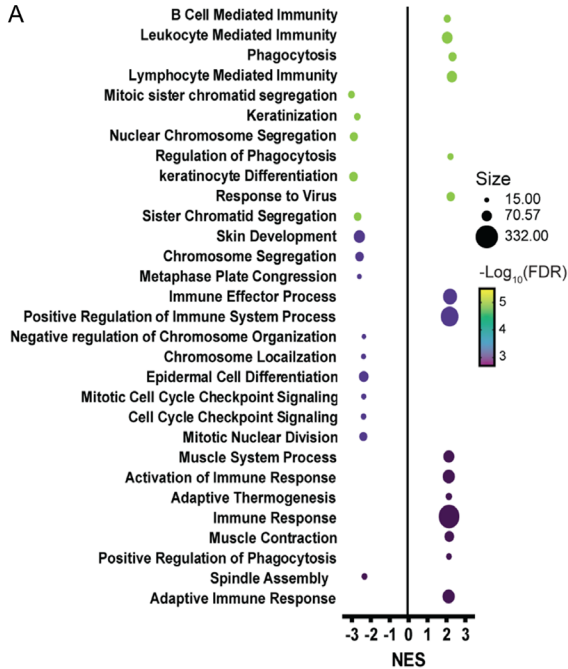
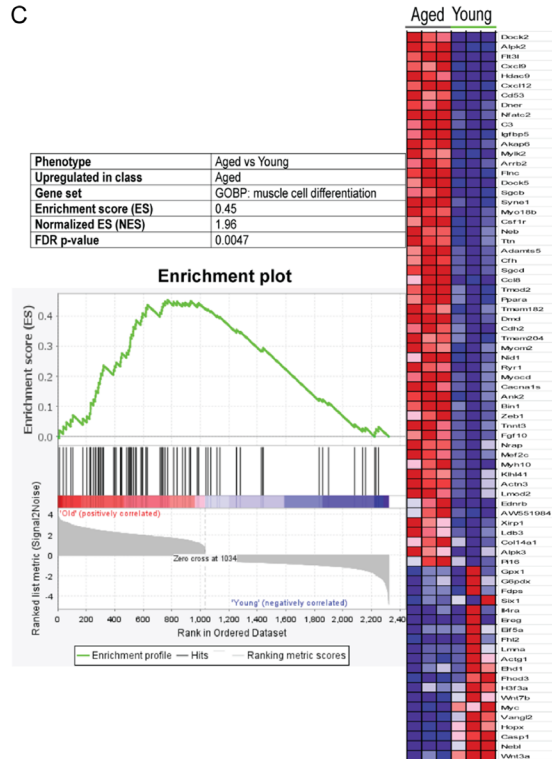
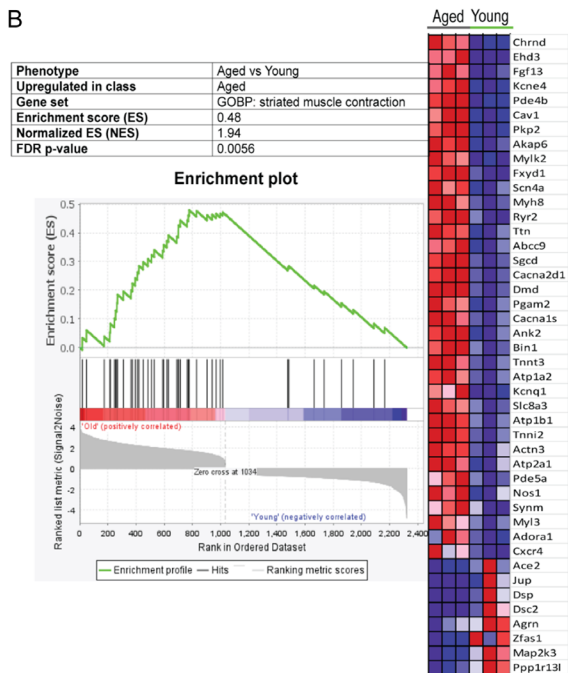


Figure 4. Gene Set Enrichment Analysis (GSEA) of the significant differentially expressed genes between aged and young mice urethra tissue. (A) The enrichment plot of the top 30 enriched gene sets filtered by FDR is displayed on the y-axis. The x-axis shows the Normalized Enrichment Score (NES) of the gene sets, where a positive enrichment score indicates upregulated gene sets, and a negative enrichment score suggests downregulated gene sets in aged mice. The diameter of the circles represents the gene size, or number of genes, in each gene set. The color indicates the $-\log_{10}(FDR)$ p-value. Example of expression levels of the specific genes in a gene set is shown in (B) and (C).



data showing the upregulation of many immune-related and muscle-specific biological processes in aged urethral tissues suggests an overall increase in activity relating to muscle growth, regeneration, and/or repair. This is an intriguing result because immune cells play a crucial role in muscle regeneration and growth [20]. This result is unexpected because downregulation of immune response in aged tissues is one of the hallmarks of aging or immune senescence

[21-24], whereas in the current study the opposite effects on the immune response were observed. Alternatively, the data could also indicate that an induction of pro-inflammatory state which leads to “muscle loss” in the aged mouse urethra.

The RNA-seq data showed tissue-specific gene sets, such as muscle-related genes. Similarly, many crucial genes essential for striated mus-

Investigating age-derived urethral dysfunction

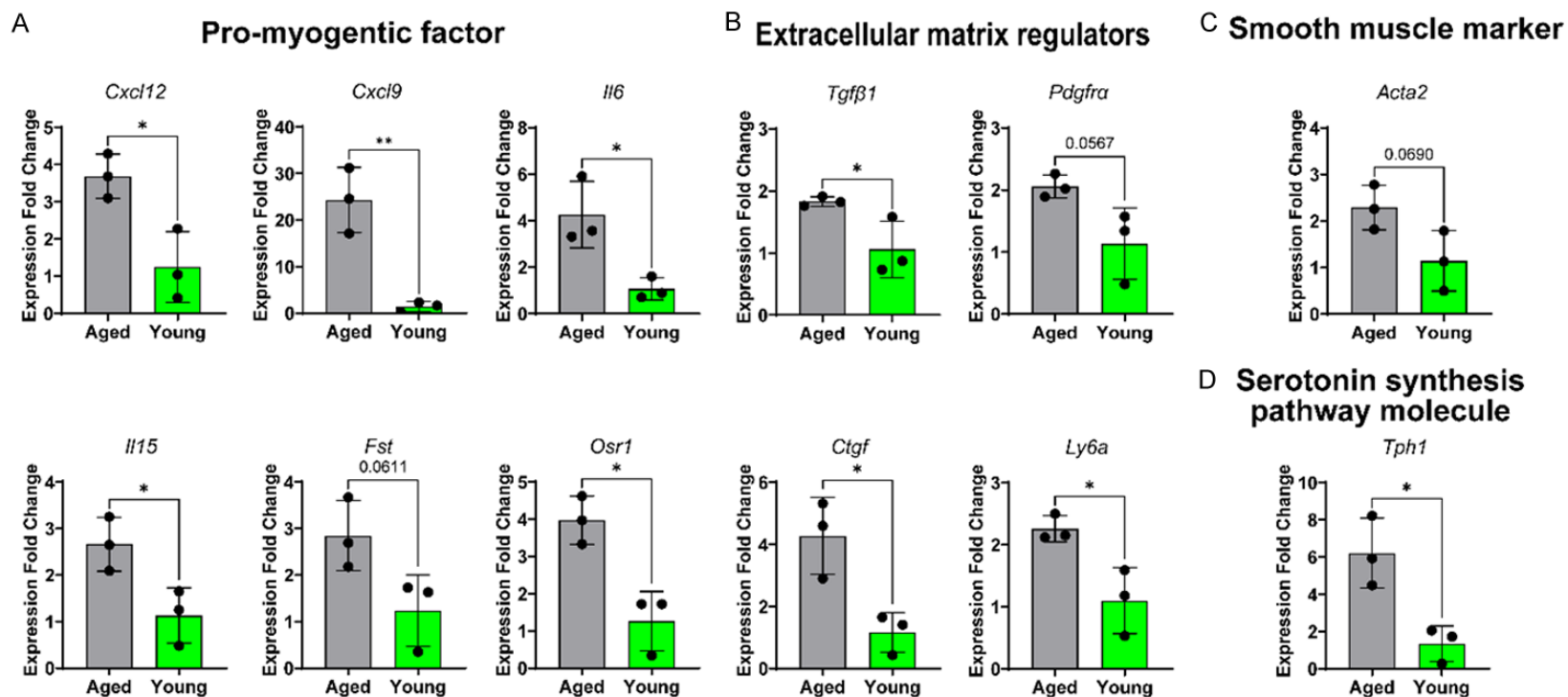


Figure 5. Validation of RNA-seq analysis via reverse transcription-quantitative Polymerase Chain Reaction (RT-qPCR). Specific genes of interest were selected to further validate the bulk RNA-sequencing data. Six pro-myogenic factors (A), four extracellular matrix regulators (B), one smooth muscle marker (C), and a serotonin synthesis pathway molecule (D) were evaluated. All RT-qPCR reactions were performed in triplicates, where the error bars illustrate standard deviations. Expression fold change was calculated based on $2^{-\Delta\Delta CT}$, where each sample was normalized to the expression of gene *Gapdh*. T-tests were performed to measure statistical significance of expression fold change between aged and young samples. All the specific genes of interest were found to be upregulated in aged mice with statistical significance, except *Pdgfr- α* , *Acta-2*, and *Fst*. Statistical significance is represented by the asterisks (*) symbol, where * represents p -value < 0.05 and ** represent p -value < 0.01.

Investigating age-derived urethral dysfunction

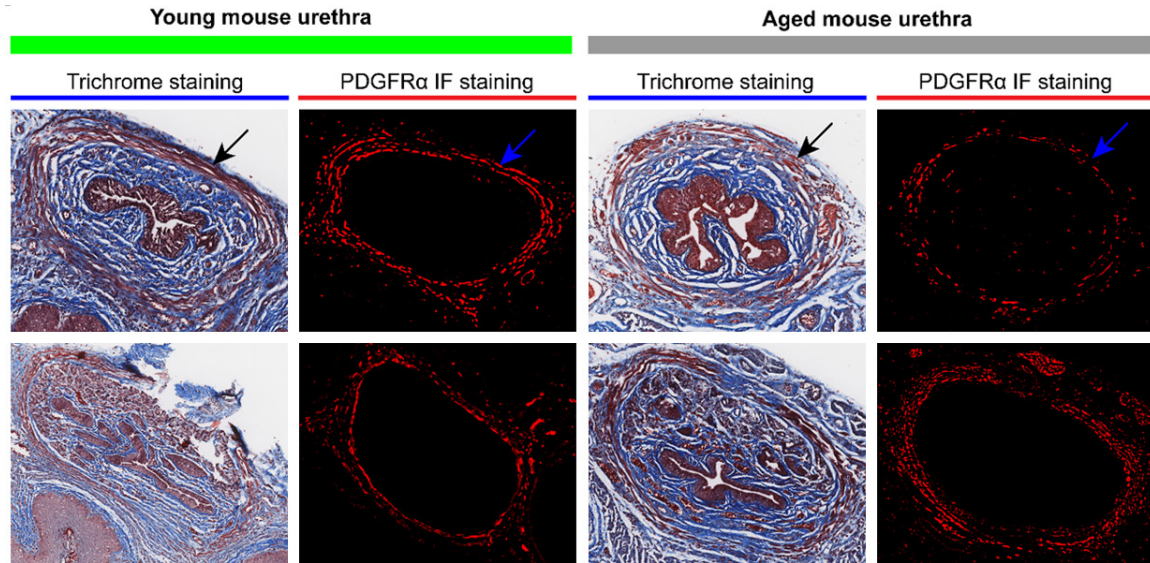


Figure 6. Immunofluorescence staining of mice female urethral tissues. Immunofluorescence staining of PDGFR α in young (left) and aged (right) mice female urethral tissues and comparing them with their trichrome stained consecutive sections demonstrates PDGFR α positive cells in the striated muscle layer of the urethra. The arrows indicate the striated muscle layer.

cle cell growth, such as *Fst*, *Acvr1*, *Il6*, *Il15*, *Cxcl12*, and *Cxcl9* are highly upregulated [25-28]. Notably, Activin A Receptor Type 1 (*Acvr1*) is a type I receptor for the TGF- β family of signaling molecules, and follistatin (*Fst*) is activin-binding protein [29-31]. Both have been shown to regulate resident stem cell populations, muscle stem cells (MuSCs) and fibro/adipogenic progenitors (FAPs) and play a functional role in muscle regeneration [29-32]. On the other hand, our immunofluorescent staining of the mid-urethral slides also demonstrated PDGFR- α cells in both young and aged mice urethra striated muscle layer. We should note that these PDGFR- α cells can demonstrate FAPs, but also, other cells of mesodermal derivatives [33].

Cxcl12 and *Cxcl9* are essential in recruitment, localization, maintenance, development, and differentiation of progenitor stem cells of the musculoskeletal system. *Il6* and *Il15* are myokines that are produced and released by myocytes or immune cells in muscle tissue in response to muscular contractions. However, paradoxically, a decreased proportion of striated muscle is seen in aging, as shown in our morphometric data. The underlying mechanisms for this observation remain unclear. Further studies using single cell analysis and spatial transcriptome profiling are therefore

warranted to identify individual cell components and differential gene expression among differential cell components between young and aged female urethral tissues.

The RNA-seq data also showed *Il33* (Interleukin-33) to be significantly downregulated in aged mouse urethra tissue (-7.79-fold change, FDR p -value = 1.01E-11) compared to the younger urethra tissue, as shown in **Figure 3B**. Kustwanto *et al.* has demonstrated the key role of *Il33* in the hemostasis of young skeletal muscle, and *Il33* deficit in poor repair of aged skeletal muscle [34]. They demonstrated administration of *Il33* regulated muscle Treg cells into the aged mice striated muscle improved the muscle regeneration in aged mice. The major *Il33* expressing cells in skeletal muscle displayed markers for FAP cells [34]. Our study demonstrated decreased *Il33* expression in aged mice urethra compared to the young urethra which is compatible with the above observation in the aged mice skeletal muscle. This raises the potential role of FAP cells as the major *Il33* expressing cells in urethra striated muscle deterioration with aging.

Connective tissue changes with advancing age, like changes in the rest of the body, could also play a role in the incontinence symptoms. However, to our knowledge, the correlation

Investigating age-derived urethral dysfunction

between extracellular matrix components in women - collagen and elastin - and urethral function has not been determined. Our study demonstrated a higher extracellular matrix connective-tissue ratio was observed in the mid-urethral striated muscle layer of aged than in younger mice. We also demonstrated the proportion of elastin containing areas in the mid-urethral striated muscle layer was lower than in the younger mice. Consistently, RNA-seq results revealed that the mRNA levels of elastin (*Eln*) were significantly lower (fold change = -1.91, FDR *p*-value = 0.03), whereas the levels of *Ctgf* mRNA, a primary mediator of TGF- β -induced fibrosis, was found to be highly upregulated in aged mice urethral tissue compared to those from young female mice. Further studies are therefore in progress to determine whether protein expression levels of elastin and CTGF were also changed with aging in the urethra.

In addition, the *Lep* gene encoding leptin, inhibits lipogenic pathways and promotes the oxidation of fatty acids in skeletal muscle, was also overexpressed in aged female urethral tissues. Collins *et al.* [35] has shown that leptin is an indispensable factor for mediated development of muscle mass and strength in mice [36]. Leptin reducing Ca²⁺ influx in the smooth muscle resulted in either inhibiting spontaneous muscle contraction or inducing muscle contractions [37]. Qin *et al.* [38] has further demonstrated that leptin-deficient B6.V-Le^{po}b/J mice exhibits obesity and high blood glucose accompanied by the urinary dysfunction phenotype. Leptin has even been considered as a novel agent to treat women with overactive bladder symptoms [37]. However, the role of leptin in urinary dysfunction remains largely unclear [39, 40]. Therefore, there is a need for understanding or clarifying the biological and functional role of leptin for changes of urethral function during aging.

Conclusion

Functional LPP measurement and morphometric analysis of the aged female mice is qualitatively similar to elderly human urethra and exhibits less striated muscle, more extracellular matrix/fibrosis, and diminished elastin fibers compared to young mice. Gene expression profiling analysis by the bulk RNA-seq of the whole urethra demonstrated immune response

and muscle-related (striated and smooth) pathways were predominantly enriched, whereas keratinization, skin development, and cell differentiation pathways were significantly down-regulated in aged urethral tissues compared to those from female young mice. Our result suggests that molecular pathways (*i.e.*, ACVR1/FST signaling and CTGF/TGF- β signaling) leading to a decreased striated muscle mass and an increase in fibrotic extracellular matrix in the process of aging warrants further studies for their roles in the declined urethral function with aging.

Acknowledgements

The University of California, Irvine Experimental Tissue Resource (ETR) performed tissue preparation, trichrome staining, and Verhoeff's Elastic Staining. Sequencing library quality control, sequencing library concentration measurement and next-generation sequencing experiments were conducted at the University of California, Irvine Genomics Research and Technology Hub (GRTH). This work was supported by departmental funding provided to Dr. Zhina Sadeghi, by the Department of Urology at the University of California, Irvine. This work was partly supported by VA merit award I01BX-005105 (to X.Z.). Dr. DeLancey and Dr. Balis had their effort supported by RC2 DK122379, and NIH.NIAMS R01NS120060 grant (to S.A.V.).

Disclosure of conflict of interest

None.

Address correspondence to: Drs. Zhina Sadeghi and Yi Xi Wu, Department of Urology, School of Medicine, University of California, 3800 W. Chapman Ave, Suite 7200, Orange, Irvine, CA 92868, USA. Tel: 714-456-6047; Fax: 1-888-378-4358; E-mail: zhinass@hs.uci.edu (ZS); yxwu@hs.uci.edu (YXW)

References

- [1] Patel UJ, Godecker AL, Giles DL and Brown HW. Updated prevalence of urinary incontinence in women: 2015-2018 national population-based survey data. *Female Pelvic Med Reconstr Surg* 2022; 28: 181-187.
- [2] Hannestad YS, Rortveit G and Hunskaar S. Help-seeking and associated factors in female urinary incontinence. *The Norwegian EPIN-*

Investigating age-derived urethral dysfunction

- CONT Study. Epidemiology of incontinence in the county of Nord-Trøndelag. *Scand J Prim Health Care* 2002; 20: 102-7.
- [3] Harris SS, Link CL, Tennstedt SL, Kusek JW and McKinlay JB. Care seeking and treatment for urinary incontinence in a diverse population. *J Urol* 2007; 177: 680-4.
- [4] Minassian VA, Yan X, Lichtenfeld MJ, Sun H and Stewart WF. The iceberg of health care utilization in women with urinary incontinence. *Int Urogynecol J* 2012; 23: 1087-93.
- [5] Daneshgari F, Kong W and Swartz M. Complications of mid urethral slings: important outcomes for future clinical trials. *J Urol* 2008; 180: 1890-7.
- [6] Trowbridge ER, Wei JT, Fenner DE, Ashton-Miller JA and Delancey JO. Effects of aging on lower urinary tract and pelvic floor function in nulliparous women. *Obstet Gynecol* 2007; 109: 715-20.
- [7] Rud T. Urethral pressure profile in continent women from childhood to old age. *Acta Obstet Gynecol Scand* 1980; 59: 331-5.
- [8] Carlile A, Davies I, Rigby A and Brocklehurst JC. Age changes in the human female urethra: a morphometric study. *J Urol* 1988; 139: 532-5.
- [9] Liu G, Daneshgari F, Li M, Lin D, Lee U, Li T and Damaser MS. Bladder and urethral function in pelvic organ prolapsed lysyl oxidase like-1 knockout mice. *BJU Int* 2007; 100: 414-8.
- [10] Barisoni L, Lafata KJ, Hewitt SM, Madabhushi A and Balis UGJ. Digital pathology and computational image analysis in nephropathology. *Nat Rev Nephrol* 2020; 16: 669-685.
- [11] Hipp JD, Cheng J, Hanson JC, Rosenberg AZ, Emmert-Buck MR, Tangrea MA and Balis UJ. SIVQ-LCM protocol for the ArcturusXT instrument. *J Vis Exp* 2014; 51662.
- [12] Smith-Anttila CJA, Morrison V and Keast JR. Spatiotemporal mapping of sensory and motor innervation of the embryonic and postnatal mouse urinary bladder. *Dev Biol* 2021; 476: 18-32.
- [13] Chandran S, Guo T, Tolliver T, Chen W, Murphy DL and McPherron AC. Effects of serotonin on skeletal muscle growth. *BMC Proceedings* 2012; 6 Suppl 3: O3.
- [14] Santini MP, Malide D, Hoffman G, Pandey G, D'Escamard V, Nomura-Kitabayashi A, Rovira I, Kataoka H, Ochando J, Harvey RP, Finkel T and Kovacic JC. Tissue-resident PDGFRalpha(+) progenitor cells contribute to fibrosis versus healing in a context- and spatiotemporally dependent manner. *Cell Rep* 2020; 30: 555-570, e7.
- [15] Li X, Long J, Liu Y, Cai Q, Zhao Y, Jin L, Liu M and Li C. Association of MTOR and PDGFRA gene polymorphisms with different degrees of myopia severity. *Exp Eye Res* 2022; 217: 108962.
- [16] van Geelen H and Sand PK. The female urethra: urethral function throughout a woman's lifetime. *Int Urogynecol J* 2023; 34: 1175-1186.
- [17] Andreescu CF, Mihai LL, Răescu M, Tuculină MJ, Cumpătă CN and Ghergic DL. Age influence on periodontal tissues: a histological study. *Rom J Morphol Embryol* 2013; 54 Suppl: 811-5.
- [18] Kadekawa K, Nishijima S, Noguchi K, Okitsu S, Karube K, Matsumoto S, Yamamoto H and Sugaya K. Deletion of the lysyl oxidase-like 1 gene induces impaired elastin fiber synthesis and inefficient urethral closure in rats. *Biomed Res* 2021; 42: 23-31.
- [19] Pipitone F, Sadeghi Z and DeLancey JOL. Urethral function and failure: a review of current knowledge of urethral closure mechanisms, how they vary, and how they are affected by life events. *Neurourol Urodyn* 2021; 40: 1869-1879.
- [20] Ziemkiewicz N, Hilliard G, Pullen NA and Garg K. The role of innate and adaptive immune cells in skeletal muscle regeneration. *Int J Mol Sci* 2021; 22: 3265.
- [21] Lavelle CL. *Applied oral physiology*. Butterworth-Heinemann; 2013.
- [22] López-Otín C, Blasco MA, Partridge L, Serrano M and Kroemer G. The hallmarks of aging. *Cell* 2013; 153: 1194-217.
- [23] Mittelbrunn M and Kroemer G. Hallmarks of T cell aging. *Nat Immunol* 2021; 22: 687-698.
- [24] Salminen A, Kaarniranta K and Kauppinen A. Inflammaging: disturbed interplay between autophagy and inflammasomes. *Aging (Albany NY)* 2012; 4: 166-75.
- [25] Gilbert W, Bragg R, Elmansi AM, McGee-Lawrence ME, Isales CM, Hamrick MW, Hill WD and Fulzele S. Stromal cell-derived factor-1 (CXCL12) and its role in bone and muscle biology. *Cytokine* 2019; 123: 154783.
- [26] Puchert M, Adams V, Linke A and Engele J. Evidence for the involvement of the CXCL12 system in the adaptation of skeletal muscles to physical exercise. *Cell Signal* 2016; 28: 1205-1215.
- [27] Nielsen AR, Mounier R, Plomgaard P, Mortensen OH, Penkowa M, Speerschnieder T, Piilegaard H and Pedersen BK. Expression of interleukin-15 in human skeletal muscle effect of exercise and muscle fibre type composition. *J Physiol* 2007; 584: 305-12.
- [28] Biferali B, Proietti D, Mozzetta C and Madaro L. Fibro-adipogenic progenitors cross-talk in skeletal muscle: the social network. *Front Physiol* 2019; 10: 1074.
- [29] Barruet E, Garcia SM, Wu J, Morales BM, Tamaki S, Moody T, Pomerantz JH and Hsiao EC. Modeling the ACVR1(R206H) mutation in hu-

Investigating age-derived urethral dysfunction

- man skeletal muscle stem cells. *Elife* 2021; 10: e66107.
- [30] Lees-Shepard JB, Stoessel SJ, Chandler JT, Bouchard K, Bento P, Apuzzo LN, Devarakonda PM, Hunter JW and Goldhamer DJ. An anti-ACVR1 antibody exacerbates heterotopic ossification by fibro-adipogenic progenitors in fibrodysplasia ossificans progressiva mice. *J Clin Invest* 2022; 132: e153795.
- [31] Reggio A, Rosina M, Palma A, Cerquone Perpetuini A, Petrilli LL, Gargioli C, Fuoco C, Micarelli E, Giuliani G, Cerretani M, Bresciani A, Sacco F, Castagnoli L and Cesareni G. Adipogenesis of skeletal muscle fibro/adipogenic progenitors is affected by the WNT5a/GSK3/beta-catenin axis. *Cell Death Differ* 2020; 27: 2921-2941.
- [32] Akita Y, Sumino Y, Mori K, Nomura T, Sato F and Mimata H. Myostatin inhibits proliferation of human urethral rhabdosphincter satellite cells. *Int J Urol* 2013; 20: 522-9.
- [33] Chandrakanthan V, Rorimpandey P, Zanini F, Chacon D, Olivier J, Joshi S, Kang YC, Knezevic K, Huang Y, Qiao Q, Oliver RA, Unnikrishnan A, Carter DR, Lee B, Brownlee C, Power C, Brink R, Mendez-Ferrer S, Enikolopov G, Walsh W, Göttgens B, Taoudi S, Beck D and Pimanda JE. Mesoderm-derived PDGFRA(+) cells regulate the emergence of hematopoietic stem cells in the dorsal aorta. *Nat Cell Biol* 2022; 24: 1211-1225.
- [34] Kuswanto W, Burzyn D, Panduro M, Wang KK, Jang YC, Wagers AJ, Benoist C and Mathis D. Poor repair of skeletal muscle in aging mice reflects a defect in local, interleukin-33-dependent accumulation of regulatory T cells. *Immunity* 2016; 44: 355-67.
- [35] Collins KH, Gui C, Ely EV, Lenz KL, Harris CA, Guilak F and Meyer GA. Leptin mediates the regulation of muscle mass and strength by adipose tissue. *J Physiol* 2022; 600: 3795-3817.
- [36] Nwadozi E, Ng A, Strömberg A, Liu HY, Olsson K, Gustafsson T and Haas TL. Leptin is a physiological regulator of skeletal muscle angiogenesis and is locally produced by PDGFR α and PDGFR β expressing perivascular cells. *Angiogenesis* 2019; 22: 103-115.
- [37] Wuntakal R, Sharma S, Kaler M and Hollingworth T. Leptin - a novel pharmacological agent for treatment of women with overactive bladder symptoms? *Med Hypotheses* 2012; 79: 856-7.
- [38] He Q, Babcook MA, Shukla S, Shankar E, Wang Z, Liu G, Erokwu BO, Flask CA, Lu L, Daneshgari F, MacLennan GT and Gupta S. Obesity-initiated metabolic syndrome promotes urinary voiding dysfunction in a mouse model. *Prostate* 2016; 76: 964-76.
- [39] Gasbarro G, Lin DL, Vurbic D, Quisno A, Kinley B, Daneshgari F and Damaser MS. Voiding function in obese and type 2 diabetic female rats. *Am J Physiol Renal Physiol* 2010; 298: F72-7.
- [40] Kapoor DS, Davila GW, Rosenthal RJ and Ghoniem GM. Pelvic floor dysfunction in morbidly obese women: pilot study. *Obes Res* 2004; 12: 1104-7.
- [41] Marino GE and Weeraratna AT. A glitch in the matrix: age-dependent changes in the extracellular matrix facilitate common sites of metastasis. *Aging Cancer* 2020; 1: 19-29.
- [42] Verzijl N, DeGroot J, Thorpe SR, Bank RA, Shaw JN, Lyons TJ, Bijlsma JW, Lafeber FP, Baynes JW and TeKoppele JM. Effect of collagen turnover on the accumulation of advanced glycation end products. *J Biol Chem* 2000; 275: 39027-31.
- [43] Du LL and Liu P. CXCL12/CXCR4 axis regulates neovascularization and lymphangiogenesis in sutured corneas in mice. *Mol Med Rep* 2016; 13: 4987-94.
- [44] Guo L, Chen S, Liu Q, Ren H, Li Y, Pan J, Luo Y, Cai T, Liu R, Chen J, Wang Y, Wang X, Huang N and Li J. Glutaredoxin 1 regulates macrophage polarization through mediating glutathionylation of STAT1. *Thorac Cancer* 2020; 11: 2966-2974.
- [45] Peng L, Lu Y, Gu Y, Liang B, Li Y, Li H, Ke Y, Zhu H and Li Z. Mechanisms of action of Lycium barbarum polysaccharide in protecting against vitiligo mice through modulation of the STAT3-Hsp70-CXCL9/CXCL10 pathway. *Pharm Biol* 2023; 61: 281-287.
- [46] Wang X, Zhao L, Fan C, Dong Z, Ruan H, Hou W, Fan Y, Wang Q, Luan T, Li P, Rui C and Zeng X. The role of IL-15 on vulvovaginal candidiasis in mice and related adverse pregnancy outcomes. *Microb Pathog* 2022; 166: 105555.
- [47] Rosas-Taraco AG, Higgins DM, Sánchez-Campillo J, Lee EJ, Orme IM and González-Juarrero M. Local pulmonary immunotherapy with siRNA targeting TGFbeta1 enhances antimicrobial capacity in Mycobacterium tuberculosis infected mice. *Tuberculosis (Edinb)* 2011; 91: 98-106.
- [48] Song K, Qing Y, Guo Q, Peden EK, Chen C, Mitch WE, Truong L and Cheng J. PDGFRA in vascular adventitial MSCs promotes neointima formation in arteriovenous fistula in chronic kidney disease. *JCI Insight* 2020; 5: e137298.
- [49] Cheng J, Zhou X, Jiang X and Sun T. Deletion of ACTA2 in mice promotes angiotensin II induced pathogenesis of thoracic aortic aneurysms and dissections. *J Thorac Dis* 2018; 10: 4733-4740.
- [50] Ikeda A, Yamamoto T, Mineshiba J and Takashiba S. Follistatin expressed in mechanical-

Investigating age-derived urethral dysfunction

- ly-damaged salivary glands of male mice induces proliferation of CD49f(+) cells. *Sci Rep* 2020; 10: 19959.
- [51] Vallecillo-García P, Orgeur M, Vom Hofe-Schneider S, Stumm J, Kappert V, Ibrahim DM, Börno ST, Hayashi S, Relaix F, Hildebrandt K, Sengle G, Koch M, Timmermann B, Marazzi G, Sassoon DA, Duprez D and Stricker S. Odd skipped-related 1 identifies a population of embryonic fibro-adipogenic progenitors regulating myogenesis during limb development. *Nat Commun* 2017; 8: 1218.
- [52] Grajales D, Vázquez P, Ruíz-Rosario M, Tudurí E, Mirasierra M, Ferreira V, Hitos AB, Koller D, Zubiaur P, Cigudosa JC, Abad-Santos F, Vallejo M, Quesada I, Tirosh B, Leibowitz G and Valverde ÁM. The second-generation antipsychotic drug aripiprazole modulates the serotonergic system in pancreatic islets and induces beta cell dysfunction in female mice. *Diabetologia* 2022; 65: 490-505.
- [53] Gamwell LF, Collins O and Vanderhyden BC. The mouse ovarian surface epithelium contains a population of LY6A (SCA-1) expressing progenitor cells that are regulated by ovulation-associated factors. *Biol Reprod* 2012; 87: 80.
- [54] Tsoutsman T, Wang X, Garchow K, Riser B, Twigg S and Semsarian C. CCN2/CTGF plays a key role in extracellular matrix gene expression in severe hypertrophic cardiomyopathy and heart failure. *Heart Lung Circ* 2013; 22: S54.

Investigating age-derived urethral dysfunction

Table S1. RT-qPCR primers

Gene	Primer sequence	Reference	
<i>Cxcl12</i>	Forward primer (5'-)	GAGAGCCACATCGCCAGAG	[43]
	Reverse primer (5'-)	TTTCGGGTCAATGCACACTTG	
<i>Cxcl9</i>	Forward primer (5'-)	GGAGTTCGAGGAACCCTAGTG	[44]
	Reverse primer (5'-)	GGGATTTGTAGTGGATCGTGC	
<i>Il6</i>	Forward primer (5'-)	GAGGATACCACTCCCAACAGACC	[45]
	Reverse primer (5'-)	AAGTGCATCATCGTTGTTCATACA	
<i>Il15</i>	Forward primer (5'-)	ATCGCCATAGCCAGCTC	[46]
	Reverse primer (5'-)	ATGAATGCCAGCCTCAGT	
<i>Tgfb1</i>	Forward primer (5'-)	GACCTGCCCTATATTTGGA	[47]
	Reverse primer (5'-)	GCCCCGGTTGTGTTGGT	
<i>Pdgfra</i>	Forward primer (5'-)	TGGCATGATGGTCGATTCTA	[48]
	Reverse primer (5'-)	CGCTGAGGTGGTAGAAGGAG	
<i>Acta2</i>	Forward primer (5'-)	CGAAACCACCTATAACAGCATCA	[49]
	Reverse primer (5'-)	GCGTTCTGGAGGGGCAAT	
<i>Fst</i>	Forward primer (5'-)	TCTTCTGGCGTGCTTCTTG	[50]
	Reverse primer (5'-)	CCTTCTCCTCCGTTTCTTCC	
<i>Osr1</i>	Forward primer (5'-)	GCACACTGATGAGCGACCT	[51]
	Reverse primer (5'-)	TGTAGCGTCTTGTGGACAGC	
<i>Tph1</i>	Forward primer (5'-)	GACCATCTCCGAGAGCTAAACAA	[52]
	Reverse primer (5'-)	AGCAAAGGGAGGTTTCTGAGGTA	
<i>Ly6a</i>	Forward primer (5'-)	GACCTGGAGGCACACAGCC	[53]
	Reverse primer (5'-)	CATGTGGGAACATTGCAGGACCCC	
<i>Ctgf</i>	Forward primer (5'-)	CCCTGCGACCCACACAAG	[54]
	Reverse primer (5'-)	TACACCGACCCACCGAAGAC	
<i>Gapdh</i>	Forward primer (5'-)	GTATTGGGCGCCTGGTCACC	[43]
	Reverse primer (5'-)	CGTCTCTGGAAGATGGTGATGG	

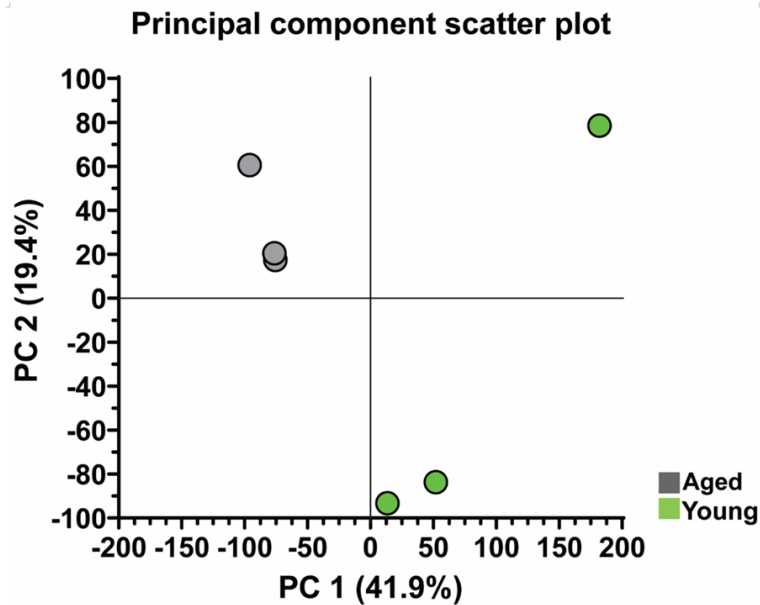


Figure S1. Principal component analysis result of RNA-seq data. The scatter plot shows the principal components (PCs) of the data. Samples with similar gene expression profiles are clustered together. Aged mice are shown in grey, and young mice are shown in Green.

Investigating age-derived urethral dysfunction

Table S2. The top 50 upregulated genes in aged mice based on bulk RNA-sequencing

Genes	Fold change	FDR <i>p</i> -value
Timp4	75.7471	4.19E-05
Pax5	65.03655	0.000458
Cd22	44.43046	1.96E-05
Jchain	41.1459	1.68E-36
Lep	40.23341	1.65E-27
Pou2af1	34.15646	1.14E-06
Tnfrsf13c	31.57357	0.004046
Cd79a	31.2026	5.71E-06
Npr3	27.76555	6.03E-30
Spib	20.7275	0.002923
Cd79b	20.43716	1.38E-05
Prol1	17.85486	1.06E-12
Ms4a4b	17.62076	0.00022
Gimap3	17.54057	0.000305
Apol11b	17.08607	0.000105
Mzb1	15.09083	0.002886
Blk	14.78111	0.004045
Bank1	14.32527	3.05E-06
Cxcr5	14.21778	0.006135
Zbtb16	13.18638	6.32E-11
Nnat	13.13806	2.92E-15
Spta1	13.09498	0.004894
Chgb	13.01848	0.006649
Fam107a	12.58617	0.008018
Acvr1c	12.54043	1.07E-10
Cxcl9	12.0247	0.0012
H2-DMb2	11.63531	0.004929
Il21r	11.60464	0.002169
H2-Ob	11.51597	0.000159
Btla	11.47376	5.18E-05
Gbp10	11.01875	5.71E-06
Cd37	10.72932	9.32E-05
C6	10.71364	6.36E-05
Nefl	9.543134	0.003096
LOC105247125	9.429319	6.41E-05
Il4i1	9.396985	0.005423
Ackr2	9.269011	0.001197
Syt1	9.256996	0.000615
Sell	9.112747	6.92E-06
Chst1	8.855918	0.007872
Ltb	8.818413	0.003439
Traf3ip3	8.814304	0.00162
Tnfrsf13b	8.805571	0.002324
Sncg	8.712145	4.47E-17
Il7r	8.54336	0.000219
Ctca1	8.524963	3.63E-09
Nefm	8.458581	0.001253

Investigating age-derived urethral dysfunction

Aqp7	8.176797	0.000878
Plscr2	8.171597	0.000435
Rasal3	8.111803	0.008313

Table S3. The top 50 downregulated genes in aged mice based on bulk RNA-sequencing

Genes	Fold change	FDR <i>p</i> -value
Krt76	-29456.9	1.03E-06
Krt16	-27760.5	2.23E-25
Kprp	-9696.39	1.09E-06
Krt6b	-4681.24	2.14E-28
Dsc1	-2062.84	8.12E-22
Dsg1a	-1946.64	4.05E-21
Uox	-1499.65	0.000482
Lor	-1495.88	5.85E-29
Krtap3-3	-1474	0.000729
Slurp1	-1463.78	0.000191
Il1f6	-1459.39	0.000229
2300002M23Rik	-1433.32	0.000169
Mt4	-1322.38	0.000333
Dsg1b	-1244.98	6.58E-25
Tgm3	-1240.45	7.74E-18
Lce3a	-1194.87	0.000277
Hrnr	-1150.19	2.6E-27
Pla2g4d	-1125.04	0.000506
Lce3e	-1102.58	0.000352
Lce1a1	-1100.19	0.000523
Lce3f	-1091.11	0.000352
Klk11	-1002.41	0.000449
Krt6a	-959.378	9.65E-29
Crct1	-948.464	2.61E-12
Teddm3	-886.108	2.22E-16
Lce1c	-871.444	0.000866
Acer1	-870.341	0.001064
Lce1g	-831.931	0.000957
Krtap3-2	-777.821	0.001943
Pla2g2f	-758.032	0.001304
Lce1d	-732.266	0.001297
Lce1e	-671.714	0.001599
Lce1i	-666.412	0.001874
Gm94	-663.086	7.15E-15
Pnpla1	-644.604	0.001296
Spink12	-635.872	0.00166
Alox12b	-580.382	8.61E-15
Them5	-568.228	1.47E-10
Serpina9	-528.088	3.52E-09
Sprr3	-523.827	1.47E-20
Calm4	-512.437	5.54E-36
Sprr1b	-495.807	8.02E-16

Investigating age-derived urethral dysfunction

Gm6557	-477.311	0.00274
Lyg1	-469.19	0.005183
Rnf222	-465.289	0.002454
Lypd5	-464.166	0.002927
St6galnac1	-443.857	0.002939
Lce1a2	-427.551	0.004279
Il1f8	-426.436	0.002557
Flg	-396.415	5.37E-39
